Experimental investigation on Iroko wood used in shipbuilding

V Bucci[1], P Corigliano[2], V Crupi[2], G Epasto[2], E Guglielmino[2] and A Marinò[1]

Abstract

The paper deals with investigations about mechanical properties of Iroko, a hardwood species used for structures in shipbuilding as glued laminated timber. Experimental tests have been carried out to assess strength, stiffness and density of Iroko in accordance with current EN Standards. All the results obtained by tensile and three-point bending tests, along with the statistical analyses performed to define the characteristics values of some mechanical properties, are reported in the paper. These values allowed to assign the strength class, reported in EN 338 Standard, to the investigated Iroko wood population. The experiments have taken into account both solid timber strips and scarf-jointed strips, in order to evaluate the influence of such a type of joint, which is widely used in wooden shipbuilding on strength and stiffness. Eventually, peculiar investigations have been carried out to analyse the failure mode of some test pieces through special experimental techniques: three-dimensional computed tomography and infrared thermography.

Keywords

Wood-based composites, computed tomography, infrared thermography, wooden ship structures, mechanical properties

Accepted: 22 September 2016

Introduction

Nowadays, there is a growing interest on wood products with the increasing progress of the quality and precision in woodworking machines.[1–4]

In the past, wood was the main construction material for shipbuilding. Certainly, wooden ships are the oldest types of ship. Today, the choice of materials for ship constructions is quite different from the past: steel, light aluminium alloys and plastic composite materials have taken over the wood. However, lately there has been a rediscovery of the wood because it represents an important natural, ecologically sustainable, flexible in usage and easy-to-process material. In fact, beside the crafts traditionally wooden built (such as fishing boats, minehunters, lobster boats, sailing yachts, junks, dhows and gondolas), there are new applications of this material for other types of vessels, such as inland/coastal passenger ships or megayachts. For instance, the hull of s/y 'Dream Symphony', which is the largest sailing yacht in the world, is built in glued laminated Iroko timber.[5] As a matter of fact, the current 'green growth' awareness in shipbuilding can be seen as the main reason for which entire wooden ships are nowadays in construction. The common wood types used in a wooden ship include both hardwood and softwood species. Hardwoods are the stronger types, coming from trees with larger leaves and shorter fibre lengths. Softwoods are obtained from trees mostly like conifers, which grow with tall, straight, single trunks with minimal branching and forking. The stronger parts of a wooden ship (i.e., the load bearing regions) are usually made from hardwoods for better strength.

The mechanical properties of timber wood depend by several factors, in particular by the wood species. The variability in the quality of timber is large, even within a selected grade of a particular species assessed by visual techniques. The choice of the wood type for a specific application in shipbuilding depends also by the country where the ship is built in order to reduce the production costs. Thus, it is crucial to know the quality and mechanical properties of the different wood species by means of experimental tests in laboratory in order to optimize their usage and to assign the specific strength class according to EN 338 Standard. Moreover, during service life

[1]Department of Engineering and Architecture, University of Trieste, Trieste, Italy
[2]Department of Engineering, University of Messina, Messina, Italy

Corresponding author:
G Epasto, Department of Engineering, University of Messina, Contrada di Dio, Sant'Agata, 98166 Messina, Italy.
Email: gabriella.epasto@unime.it

performances of the structural timber could be affected by alterations due to biological decay or mechanical damage, so non-destructive testing techniques are also very useful. An overview of non-destructive testing methods for wood-based materials is reported in Niemz and Mannes.[6]

The present paper deals with a research on the mechanical characterization of a hardwood species that has been adopted for a sailing giga-yacht. Specifically, experimental investigations on Iroko solid timber with and without scarf-joints have been carried out. Iroko is not the type of wood prevalent or dominant in shipbuilding, but there are some applications, and so it is important to know its mechanical properties. Iroko wood is more often used in shipbuilding not as solid timber but as laminate. The mechanical characterization of Iroko timber is the first step to assess the mechanical properties of Iroko wood laminates by means of theoretical approaches based on the Classical Lamination Theory. This was the motivation of this study. There are different types of joints in the wooden structures (for instance, finger joints and scarf joints), but the scarf joints are the most used for wooden boats, so they were investigated in this study. The failure mode of the investigated test pieces has been investigated using two experimental techniques: three-dimensional (3D) computed tomography (CT) and infrared thermography (IRT).

The CT has been already applied by the authors for analysing the impact responses of both laminated and sandwich composites,[7–9] but there are few applications to wood. The X-ray CT method was used by Li et al.[10] to measure the moisture content in wood and wood-based products. Paris and Kamke[11] used micro X-ray computed tomography (XCT) to analyse the 3D adhesive penetration behaviour of different wood–adhesive bondlines.

The application of IRT for the analysis of materials during mechanical tests has attracted wide attention during the last years. It is well known that a metallic specimen changes its temperature when it is subjected to cyclic stresses. If the strain is elastic, the temperature change is produced by two main effects: elasto-plasticity and thermoelasticity. Both the effects can be detected by means of an IR camera.[12] IRT was applied for the analysis of different materials subjected to different loading conditions: laminated and sandwich composites under impact loading,[9] laminated composites under tensile static loading,[13] steel welded joints[14] and shape memory alloys[15] under fatigue loading. However, there are few studies[16–21] in literature on the IRT application to wood. Thermography is a non-contact and non-destructive technique, which could be used for in situ inspections of wooden structural members of ships for surveying surface defects, zones with different moisture content and to detect different wood species through their density.[16]

Broadly, IRT can be classified either as passive or active. In passive thermography, the temperature of the object under investigation is detected without any external heat stimulation because the object itself acts as a source of heat, while external heat stimulation is essential for active thermography experiments. Both categories can be used for thermographic investigations of wood.[17] The active thermography is generally advisable for defects detection, but it is very hard to classify the internal defects.[18] Lopez et al.[18] applied the active IRT for the detection of singularities and subsurface defects in wood. Lock-in thermography, which is an active IRT, can be used for detecting glue deficiency in laminated wood as demonstrated by Berglind and Dillenz.[19] Passive thermography, instead, can be applied to detect moisture content in wood.[20] Lopez et al.[21] used IRT to monitor the evolution of the temperature over time and designed a procedure for the estimation of wood density, which is one of the most important physical characteristics of timber because it gives a general indication of its quality.

The novelty of the present investigation is the IRT application for the temperature detection during 41 static tensile tests carried out on Iroko wood specimens with and without scarf joints.

Tensile tests on solid and scarf-jointed timber strips

With reference to both solid timber and scarf-jointed timber strips, a series of tensile tests has been carried out in accordance to EN 408 to determine the modulus of elasticity $E_{t,0}$ and the maximum strength $f_{t,0}$ in tension parallel to grain. Through two different types of specimens, it is possible to highlight the influence of the scarf joint on the mechanical characteristics of the lamina.

Figures 1 and 2 show the geometry and the nominal dimensions of the test pieces used.

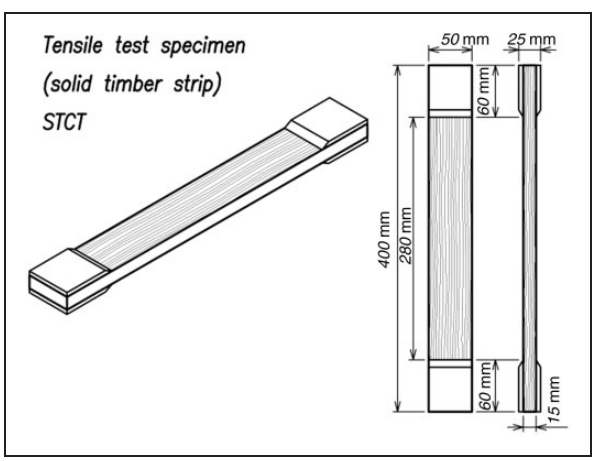

Figure 1. Tensile test specimen geometry (solid timber strip).

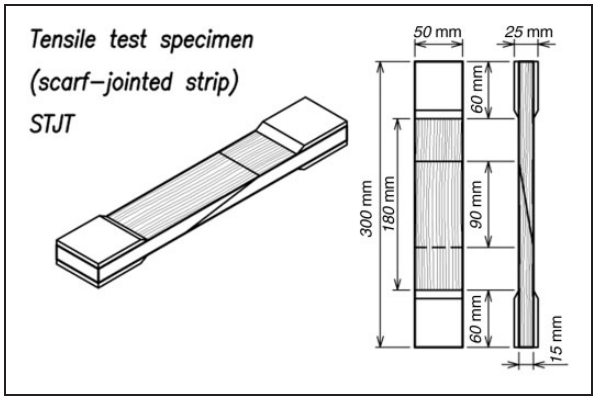

Figure 2. Tensile test specimen geometry (scarf-jointed strip).

The solid timber specimens are made of a single longitudinal-oriented lamina with tabs at the ends in order to protect the specimen from being crushed by the grip mechanism of the test machine. The scarf-jointed specimens are similar to the previous ones, but present a scarf joint in the middle part characterized by a bevel ratio 6:1 (length to thickness ratio) of the joined region in order to assure an adequate area of the adhesive. The adhesive used is an epoxy resin which is widely used for boatbuilding applications.

The weight of the test pieces was measured by a precision balance, and, taking into account their mean volume, a mean density was obtained for both the solid timber (622 kg/m^3) and the scarf-jointed strips (616 kg/m^3). The moisture content was measured for each wood specimen by a TRAMEX Moisture Encounter Plus, and the same mean value of 14% resulted for both types of specimens.

The tensile load F was applied at a constant rate (4 mm/min) with a preload of 10 kN without inducing bending. In compliance with EN 408 Standard, the loading rate was chosen in order to reach the maximum load within 5 min. In order to assess the Young modulus $E_{t,0}$, the displacements were measured during the tests using an extensometer with a gage length l_0 equal to 100 mm.

According to EN 408, the tensile strength $f_{t,0}$ is given by the equation

$$f_{t,0} = \frac{F_{max}}{A} \tag{1}$$

where F_{max} is the maximum load during the test and A is the area of the initial cross section of the test piece.

The modulus of elasticity in tension $E_{t,0}$ is given by the equation

$$E_{t,0} = \frac{l_0(F_2 - F_1)}{A(w_2 - w_1)} \tag{2}$$

where l_0 is the reference length (mm), $(F_2 - F_1)$ represents the load increment (N) on the straight line portion of the load–displacement curve and $(w_2 - w_1)$ the corresponding increment of displacement (mm). For each test, the domain $(w_2 - w_1)$ has to be chosen in order to get a simple linear regression of the loads with a coefficient of determination R^2 greater than 0.99.

Table 1. Tensile test results for solid timber strips.

Specimen	$E_{t,0}$ (N/mm^2)	$f_{t,0}$ (N/mm^2)
STCT 16	13,798	40.5
STCT 24	15,300	40.5
STCT 25	14,845	49.8
STCT 26	13,913	38.2
STCT 27	10,826	28.5
STCT 28	12,101	35.0
STCT 29	16,144	47.5
STCT 30	11,629	34.1
STCT 31	11,437	29.8
STCT 32	12,539	38. 8
STCT 33	12,003	37.6
STCT 34	10,934	32.1
STCT 35	13,119	38.5
STCT 36	12,879	44.3
STCT 37	14,616	46.1
STCT 38	12,040	37.6
STCT 39	14,219	38.4
STCT 40	12,342	39.6
STCT 41	13,934	39.0
STCT 42	11,156	29.9
STCT 46	13,526	38.8

Tables 1 and 2 show the results obtained in the tensile tests for the solid timber strips and for the scarf-jointed strips, respectively. The specimens were designed using an alphanumeric label. The letters define the specimen type (with or without scarf joints) and test type (tensile or bending tests), while the numbers define the specific specimen.

A statistical analysis in accordance to EN 384 has been carried out on the basis of the test results. In particular, the characteristic values of both tensile strength $f_{t,0,k}$ and tensile modulus of elasticity $E_{t,0,k}$ have been determined as the 5-percentile value of the corresponding normal distribution. The complete procedure used to determine the Young modulus is described in more detail in the Appendix 1 'Statistical analysis of the tensile Young modulus'. In general, if $\bar{x}$ represents the mean value and RMS the root mean square of the statistical distribution, the characteristic value $x_{k,05}$ is simply given by the expression

$$x_{k,05} = \bar{x} - 1.645\ RMS \tag{3}$$

Figures 3 and 4 show the results obtained from the statistical analysis of the mechanical characteristics $E_{t,0}$ and $f_{t,0}$ for the two types of strips examined.

Table 2. Tensile test results for scarf-jointed strips.

Specimen	$E_{t,0}$ (N/mm^2)	$f_{t,0}$ (N/mm^2)
STJT 21	11,444	33.1
STJT 22	14,364	39.2
STJT 23	12,948	31.8
STJT 24	11,602	40.0
STJT 25	15,375	46.9
STJT 26	12,756	37.4
STJT 27	12,051	37.9
STJT 28	14,486	38.0
STJT 29	13,382	44.8
STJT 30	15,112	48.7
STJT 31	11,001	31.4
STJT 32	13,715	43.9
STJT 33	11,823	35.4
STJT 34	12,795	31.3
STJT 35	11,362	26.6
STJT 36	12,312	35.1
STJT 37	11,115	31.9
STJT 38	10,993	29.1
STJT 39	13,623	36.0
STJT 40	11,888	41.3

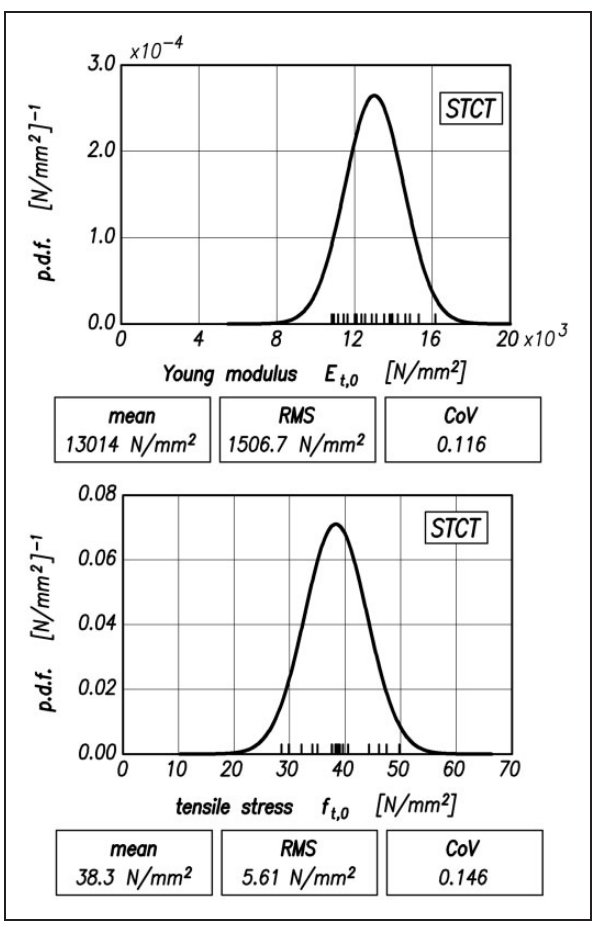

Figure 3. Statistical analysis of tensile test results (solid timber strip).

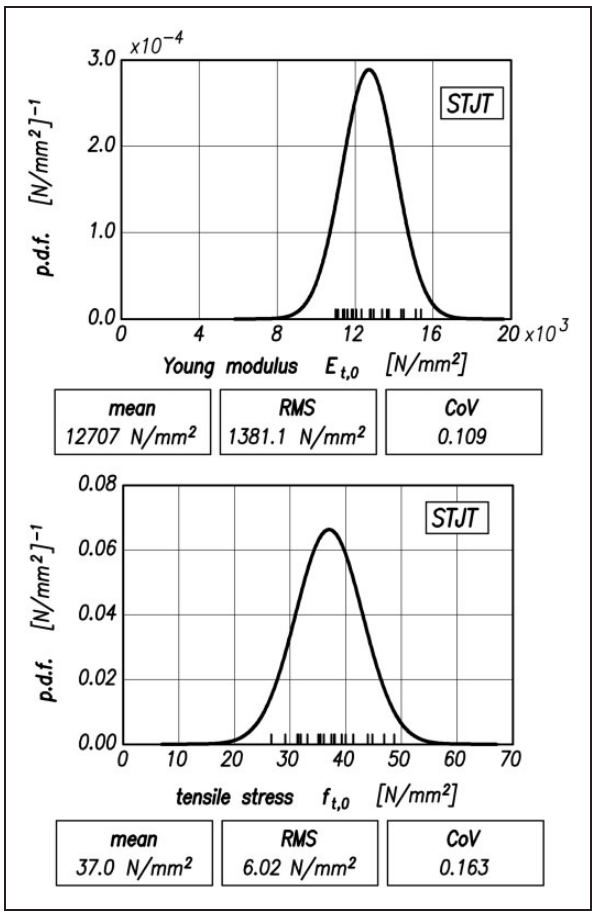

Figure 4. Statistical analysis of tensile test results (scarf-jointed strip).

Table 3. Characteristic values of the tensile test results.

Specimen	$E_{t,0,k}$ (N/mm^2)	$f_{t,0,k}$ (N/mm^2)
Solid timber strip (STCT)	10,535	29.1
Scarf-jointed strip (STJT)	10,435	27.1

The characteristics values of the tensile Young modulus and the tensile strength for solid timber and scarf-jointed timber are compared in Table 3. As can be seen, the presence of the scarf joint produces a very small decrement of the mechanical properties: about 0.95% for the elastic modulus and 6.9% for the strength.

In order to detect the failure mode, an infrared camera was used during some tests to measure the surface radiometric temperature. A SC 7200 FLIR Systems equipped with a 320×256 pixels InSb focal plane array cooled detector working in the MWIR (2.5–5 μm) spectral band (NETD typical 20 mK at 30 °C), and with a 50-mm focal length lens (FOV $11 \times 8.8°$) was used. The camera was placed at a distance of about 500 mm in front of the specimen, focusing its side view. The thermographic images were acquired at a frame rate of 160 Hz by Altair software and post-processed by means of FLIR

Systems ResearcherIR Max with DDE algorithm and frame subtraction. The environmental conditions are the following: the room temperature of the laboratory during the tests was about 20 °C and the relative humidity was about 30%. The wood specimens were painted back in order to increase their emissivity to a value equal to 0.93. Every punctual reflection and the so-called 'Narcissus effect' were eliminated by moving the IR camera. Non-uniformity correction (NUC^{TM}) calibration was carried out after adjusting focus, setting temperature range (5 °C–300 °C) and integration time (0.6 ms).

Two thermographic images of specimens (STCT and STJT) before the failure along with the thermal paths during the test are shown in Figure 5. From the analysis of the thermal path, it can be observed that small and local temperature increments are associated to local fibre breakage without the complete failure of the specimen.

The failure of the specimen occurs with a clear temperature increment of about 11 °C for the solid timber strip and about 25 °C for the scarf-jointed strip. It is worth to note that the glue of the scarf joint does not break nor shows temperature increment. The higher failure temperature of the scarf-jointed strip respect to the one of the solid timber strip depends on the presence of the adhesive, which has thermal properties different respect to the wood. The adhesive works well and is able to transfer load to the adjacent wood without affecting its mechanical properties. The IR analyses confirmed that a good penetration bondlines was reached. Indeed, during the tensile test, the temperature of the glue and of the region adjacent to the interface did not show a significant increment; thus, stress concentrations were avoided and a good transition of mechanical properties between the adhesive and the wood was obtained, ensuring a good stress transfer.

Some STJT specimens were scanned in the zone of the scarf joint using a 3D CT System Y.CT Vario. This unit is equipped with an X-ray source having maximum voltage and current of 225 kV and 7.1 mA, respectively. The detector system is a flat panel with a resolution of 1920×1536 pixel. The system, based on a variable focal-spot size technology, creates the cross-sectional images of three-dimensional objects using X-rays. A conical X-ray beam scanned the specimen, which was rotated at increments of 0.5°/s until a full rotation of 360° was achieved. A volumetric representation of the specimen to be inspected was obtained as a result of the CT. By means of tomographic analysis, both the inner and outer structures of the material along with its dimensions can be detected. Moreover, the CT system allows the detection of possible defects inside the glue (scan parameters: focal spot size 250 μm; 1-mm Cu filter; cube pitch = 50 μm; spatial resolution: 2048×2048 pixel). Figures 6 and 7 show the tomographic analyses of a scarf joint, confirming that the CT system is a useful tool for the defect detection in wood.

Quality control of the glue revealed a certain amount of pores, but a constant thickness (mean value 0.5 mm) and a good penetration inside the wood grains (Figure 7(c) to (e)) The volume of the glue measured by CT analysis is 1600 mm^3. The effective volume of the glue, measured by CT analysis, is different with respect to the designed one, which can be evaluated by the glue dimensions shown in Figure 2 and is equal to about 2281 mm^3. The difference between the measured and designed volumes of the glue does not affect the mechanical strength. Due to the porous nature of the wood, the analysis of the glue by means of CT technique allows to do the following considerations: only in few fibres, there is excessive penetration of the glue near the interface and the adhesive is well distributed, avoiding inefficient load transfer and unwanted consumption of resin. This confirms that the choice of such adhesive is appropriate, mainly in terms of surface preparation and glue viscosity. Moreover, in 3D CT analyses, no cracks were observed in the bondlines, as generally can happen to brittle adhesives.

Three-point bending tests on solid timber strips

The various species of structural timber can be usefully included in a strength class system, where different types of wood are grouped in a same class if have similar mechanical properties and density. In such a manner, species belonging to the same class can be interchangeable with regard to structural calculations. About this, the EN 338 Standard provides for a number of strength classes with reference to both softwood and hardwood species. Each class is designated with the value of the bending strength expressed in N/mm^2 and reports additional strength properties, stiffness properties and density.

In order to allocate a certain structural timber to a strength class, its characteristic values of bending strength $f_{m,k}$ and density ρ_k must be equal or greater than the values indicated in EN 338 Standard, moreover its mean modulus of elasticity in bending parallel to grain $E_{m,mean}$ (or $E_{0,mean}$) must be equal or greater than 95% of the value for that strength class.

Therefore, the definition of the strength class for Iroko timber essentially requires three series of experimental measures for establishing through a statistical analysis density, maximum stress and Young modulus in bending.

The specimens used for the bending tests are made of solid timber strip. The geometry and the nominal dimensions are shown in Figure 8.

The dimensions of 40 test pieces and their weights were measured and were determined a mean density $\rho_{mean} = 610\,\text{kg/m}^3$ with a $RMS = 34.1\,\text{kg/m}^3$, so the

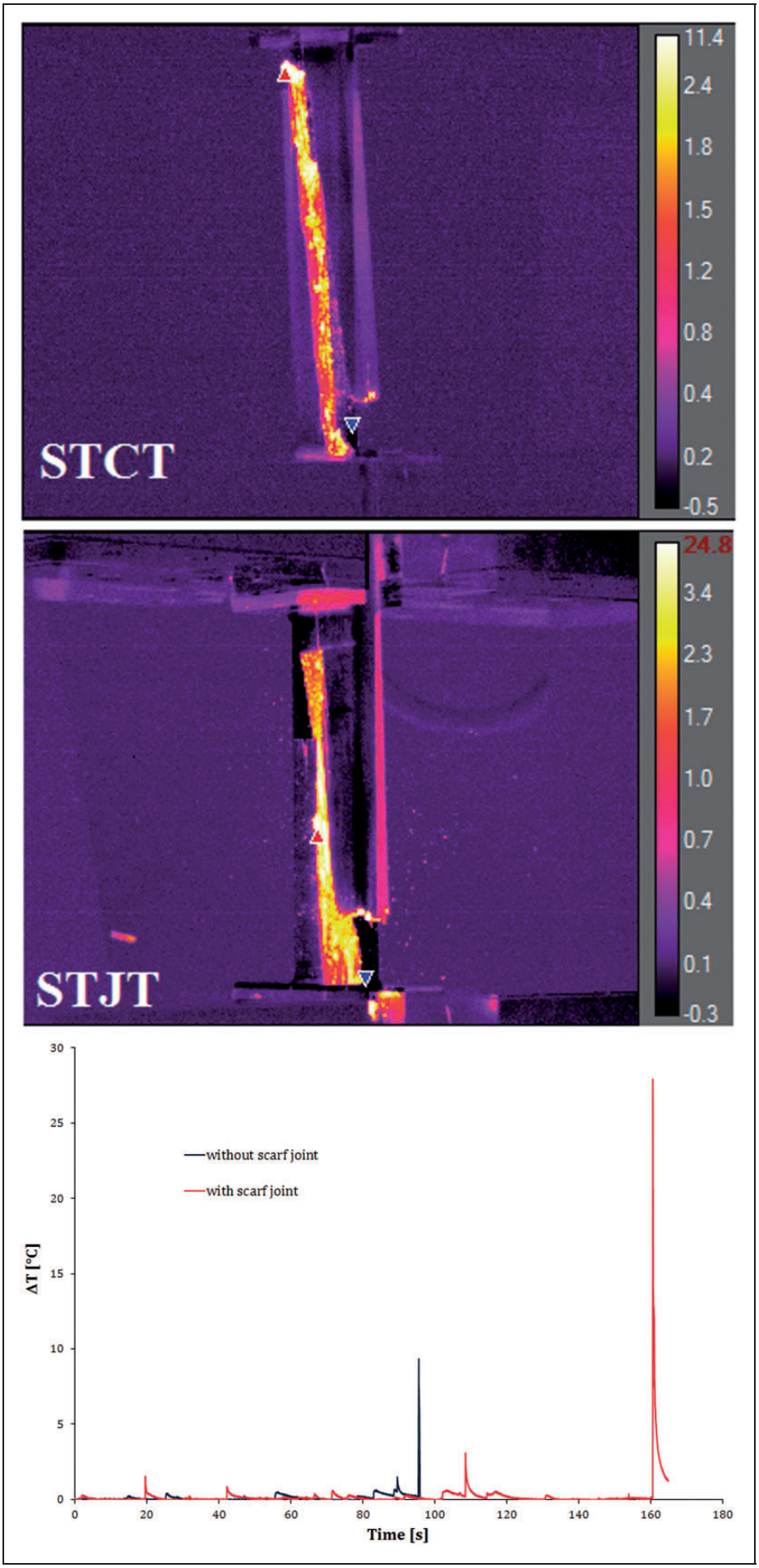

Figure 5. Thermographic images of specimens before the failure and thermal paths.

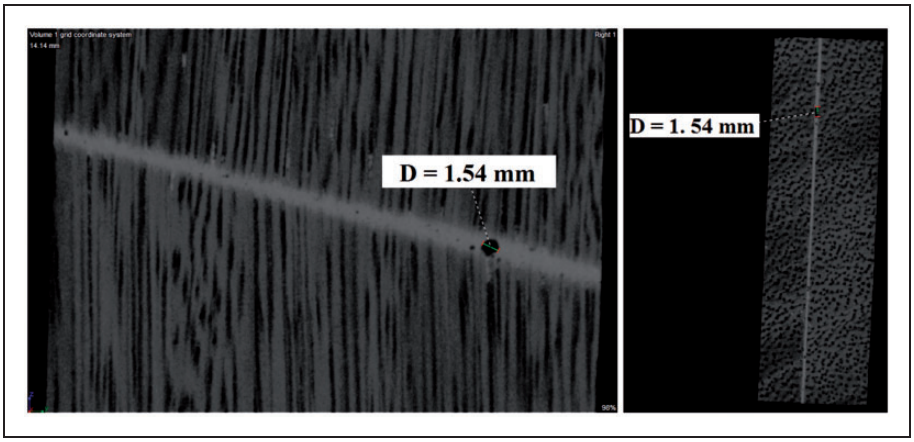

Figure 6. Quality control of the glue by CT analysis of a scarf joint.

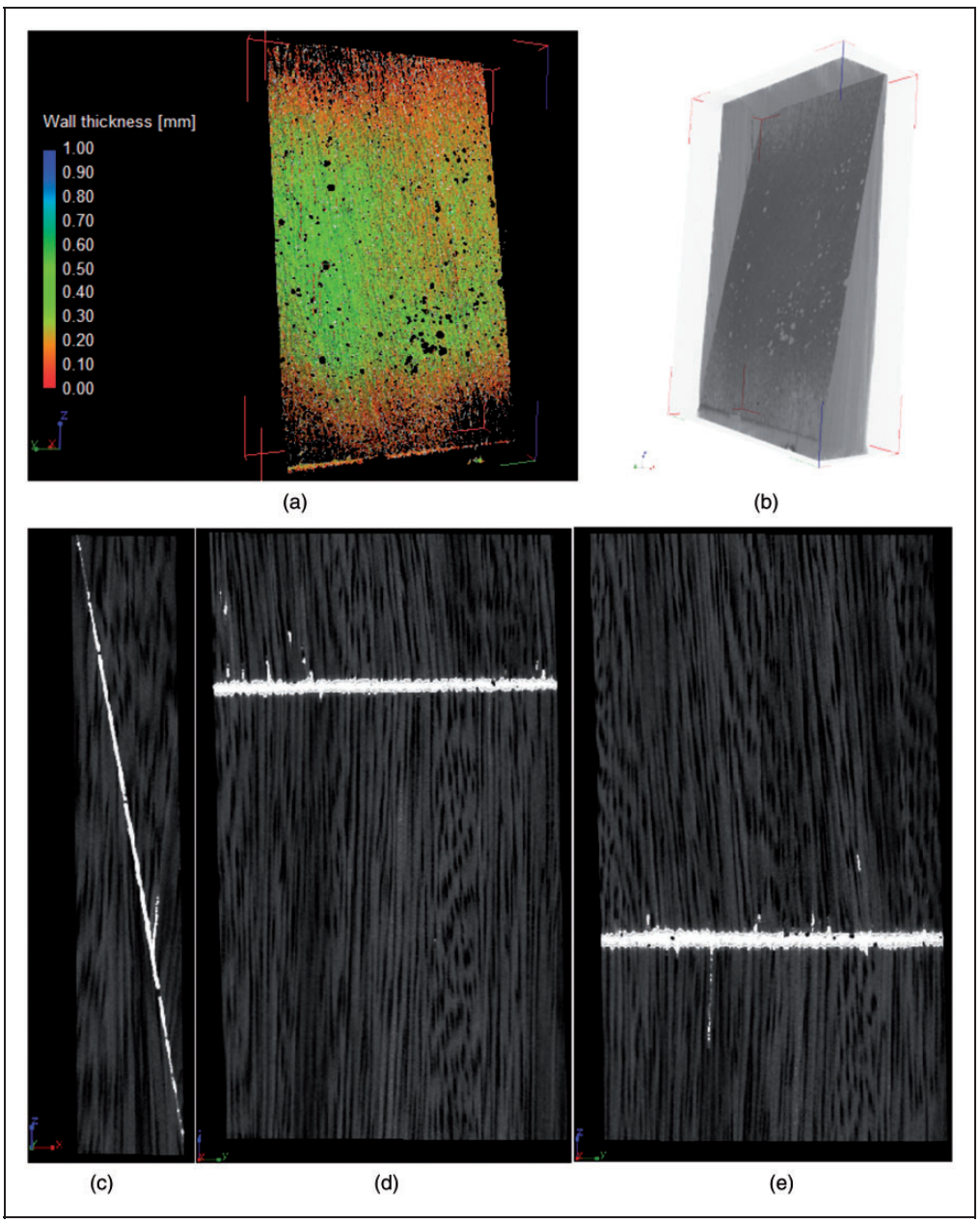

Figure 7. Wall thickness and porosity control of the glue by CT analysis of a scarf joint.

corresponding characteristic value (5-percentile) was $\rho_k = 553\,\mathrm{kg/m^3}$.

The mean moisture content was evaluated equal to 15%.

A series of three-point bending tests were carried out on 30 test pieces at a fixed support span ($l = 420\,\mathrm{mm}$) until failure in order to determine the characteristic bending strength $f_{m,k}$. The tests were performed with a preload of 10 kN and at a constant rate equal to 3 mm/min, in order to reach the maximum load F_{max} within 5 min in compliance with EN 408 Standard. The failure of the test pieces under bending loading started at the bottom surface loaded in tension, as shown in Figure 9.

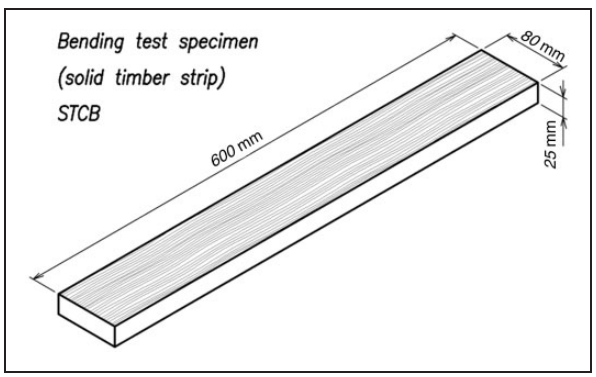

Figure 8. Bending test specimen geometry (solid timber strip).

The bending strength f_m is evaluated by the equation

$$f_m = \frac{3}{2}\,\frac{F_{max}\,l}{b\,h^2} \tag{4}$$

where b is the breadth and h is the thickness of the bending specimen.

The results obtained from the three-point bending tests carried out until failure are reported in Table 4, whereas in Figure 10 are shown the results of the statistical analysis concerning the bending stress. The characteristic value (5-percentile) of the bending strength turns to be $f_{m,k} = 71.7\,\mathrm{N/mm^2}$.

The 'method of variable support span' as specified in EN 408 Standard with reference to three-point bending tests allows to determine the modulus of elasticity in bending parallel to grain E_m (or E_0) as well as the shear modulus G by non-destructive tests. The maximum applied load is always below the proportional limit load, which is previously determined by a

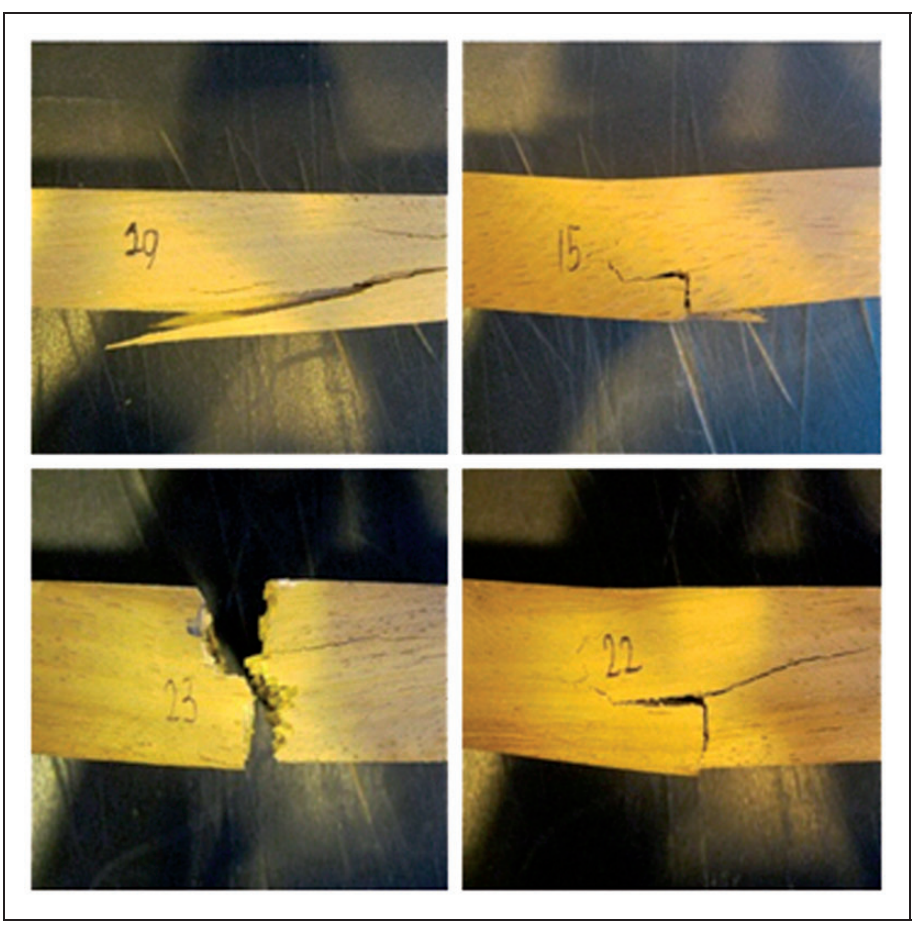

Figure 9. Failure of the test pieces under bending loading.

Table 4. Bending test results until failure ($l = 420$ mm).

Specimen	F_{max} (N)	f_m (N/mm^2)
STCB15	6170.0	77.7
STCB16	7308.4	92.1
STCB17	6686.0	84.2
STCB18	8132.1	102.5
STCB19	6803.0	85.7
STCB20	7001.3	88.2
STCB21	8238.7	103.8
STCB22	6498.6	81.9
STCB23	8679.8	109.4
STCB24	6639.2	83.7
STCB25	6646.8	83.8
STCB26	9143.3	115.2
STCB27	6511.9	82.0
STCB28	5738.3	72.3
STCB29	6794.5	85.6
STCB30	6752.7	85.1
STCB31	7079.8	89.2
STCB32	7055.5	88.9
STCB33	7592.2	95.7
STCB34	8973.1	113.1
STCB35	6093.0	76.8
STCB36	7532.1	94.9
STCB37	7540.9	95.0
STCB38	6277.3	79.1
STCB39	6308.6	79.5
STCB40	6384.7	80.4
STCB41	6784.3	85.5
STCB42	6556.1	82.6
STCB43	8077.7	101.8
STCB44	7685.9	96.8

bending test carried out until failure on a similar specimen. During the bending test, applied loads F and midspan deflections w are properly measured.

In the three-point bending test, the specimen is subjected to bending moment and shear force, so that the midspan deflection is due to the contribution of both the loading types

$$w = w_b + w_s = \frac{1}{48}\frac{F\,l^3}{E_m\,J} + \frac{1}{4}\frac{F\,l}{G\,A/\alpha} \tag{5}$$

where $J = bh^3/12$ is the second moment of area about the neutral axis, $A = bh$ the cross-sectional area, and α the form factor equal to 1.2 for any rectangular cross section.

The midspan deflection can be considered obtained only by the bending loading, and the so-called apparent modulus of elasticity $E_{m,app}$ is introduced

$$w = w_b + w_s = \frac{1}{48}\frac{F\,l^3}{E_{m,app}\,J} \tag{6}$$

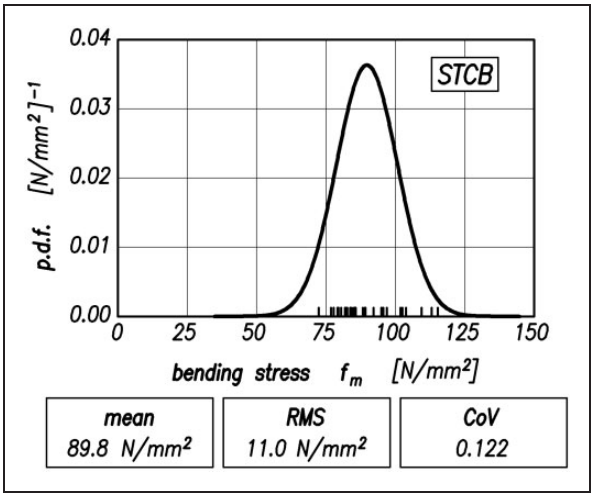

Figure 10. Statistical analysis of bending strength results.

From the comparison of equations (5) and (6), taking into account the expressions for J and A, results the following relationship for the apparent modulus of elasticity $E_{m,app}$

$$\frac{1}{E_{m,app}} = \frac{1}{E_m} + \frac{\alpha}{G}\left(\frac{h}{l}\right)^2 \tag{7}$$

Thus, a linear relationship between $1/E_{m,app}$ and $(h/l)^2$, where α/G is the slope of the straight line and $1/E_m$ is the intercept can be observed.

The 'method of variable support span' stems just from such a circumstance. Indeed, if some bending tests are carried out at different support span l (i.e., different $(h/l)^2$), and for each span, the value of $E_{m,app}$ is obtained from the F-w data (by a regression analysis in the linear range of the curve), it is possible to trace a linear regression line in the $(h/l)^2-(1/E_{m,app})$ plane that allows the evaluation of both E_m and G.

Nine specimens were used for the non-destructive bending tests. Each specimen was tested with four different support span ($l = 420$, 216, 162 and 134 mm) in order to obtain values of $(h/l)^2$ in the range between 0.0025 and 0.0350 in accordance with EN 408 Standard. For each span, the F-w curve was acquired and the apparent modulus $E_{m,app}$ determined.

The results of the calculations drawn from the 'method of variable support span' are reported in Table 5, while in Figure 11 are shown the regression straight lines from which the bending moduli E_m and the shear moduli G have been evaluated. The obtained results are summarized in Table 6. Moreover, Figure 12 shows the results of the statistical analysis inherent E_m and G. Their characteristic values (5-percentile) come to be $E_{m,k} = 10823$ N/mm^2 and $G_k = 330$ N/mm^2.

In order to establish to which strength class can be assigned to the investigated Iroko timber in accordance with EN 338 Standard, it is necessary to compare the mechanical properties values obtained from

Table 5. Results of bending tests by the variable span method.

Span l (mm)	420	216	162	134
Specimen	$E_{m,app}$ (N/mm^2)			
STCB5	10,454	8208	6313	4890
STCB6	9359	7439	5937	4611
STCB7	13,008	9647	7160	5361
STCB8	10,903	8590	6555	5160
STCB9	12,817	9451	6995	5362
STCB11	10,255	8200	6358	4903
STCB12	13,064	9595	7222	5355
STCB13	11,433	8833	6733	5238
STCB14	12,358	9292	6804	5172

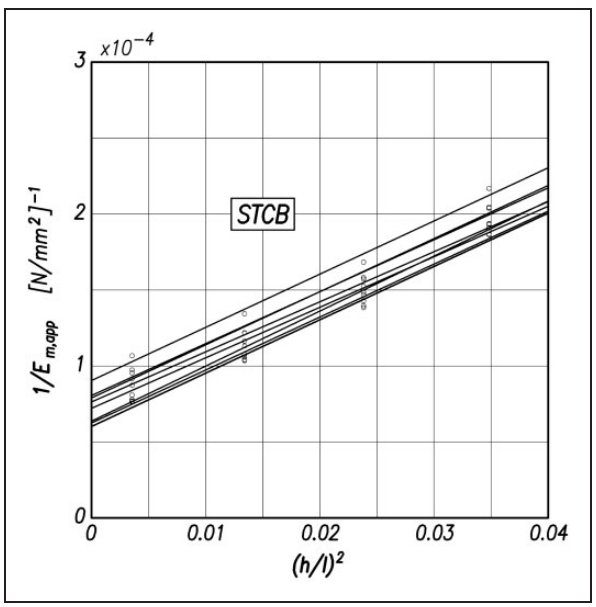

Figure 11. Linear regression analysis of variable span method data.

Table 6. Results of the regression analyses.

Specimen	E_m (N/mm^2)	G (N/mm^2)
STCB5	12,639	344
STCB6	11,051	343
STCB7	16,567	341
STCB8	13,083	365
STCB9	16,006	344
STCB11	12,391	352
STCB12	16,614	342
STCB13	13,841	361
STCB14	15,677	331

experiments with the ones reported in the Standard. Specifically, the values of $f_{m,k}$, $E_{m,mean}$ and ρ_k must be taken into consideration. The comparison shows that the strength class of Iroko is D40. Table 7 compares

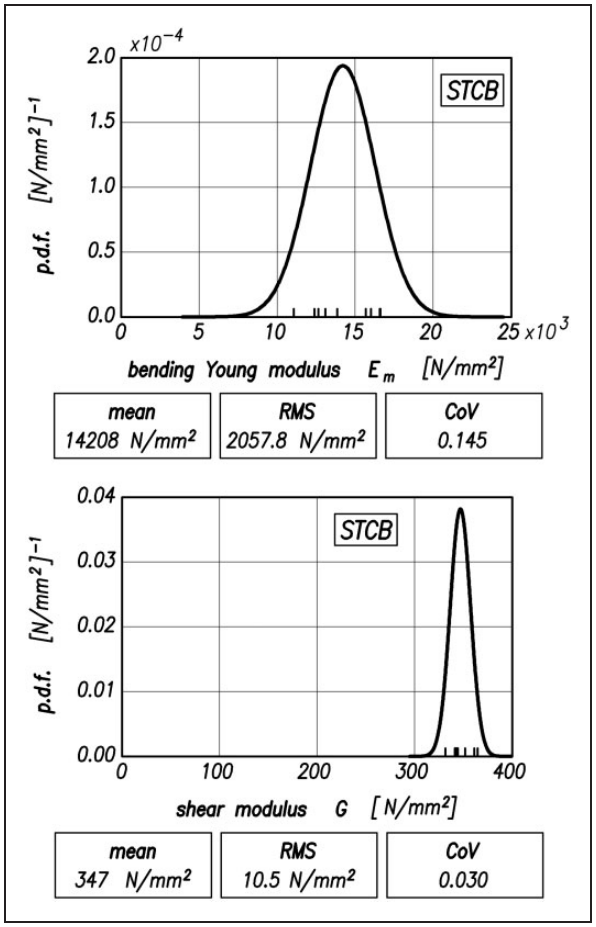

Figure 12. Statistical analysis of three-point bending tests (variable span method).

Table 7. Comparison between D40 values and experimental results.

	f_m (N/mm^2)	$E_{m,mean}$ (N/mm^2)	ρ_k (kg/m^3)
D40 strength class	40	13,000	550
Experimental results	71.7	14,208	553

the values obtained by our experimental investigation with those required for the D40 strength class.

Conclusions

- Tensile and three-point bending tests have been carried out in compliance with the current EN Standards in order to assess the mechanical properties of Iroko wood.
- The results of the tensile tests were compared with those obtained for scarf-jointed panels, demonstrating that the presence of the joint produces a very small decrement of the mechanical properties.
- The heating of the adhesive, detected by IRT, demonstrates that the adhesive works well and is able to transfer load to the adjacent wood.

- The quality control of the glue by means of CT revealed a certain amount of pores, but a constant thickness and a good penetration inside the wood grains.
- Statistical analyses were performed to the results of the bending tests in order to define the characteristics values of some mechanical properties by which it is assigned the pertinent structural strength class to the investigated Iroko wood population according to EN 338 Standard.
- The 'method of variable support span', as specified in EN 408 Standard with reference to three-point bending tests, allowed to determine the modulus of elasticity in bending parallel to grain and the in-plane shear modulus.

Declaration of Conflicting Interests

The author(s) declared no potential conflicts of interest with respect to the research, authorship, and/or publication of this article.

Funding

The author(s) received no financial support for the research, authorship, and/or publication of this article.

References

1. Lucisano G, Stefanovic M and Fragassa C. Advances design solutions for high-precision woodworking machines. *Int J Qual Res* 2016; 10: 143–158.
2. Fotouhi M, Saghafi H, Brugo T, et al. Effect of PVDF nanofibers on the fracture behavior of composite laminates for high-speed woodworking machines. *Proc IMechE, Part C: J Mechanical Engineering Science*. Epub ahead of print 13 May 2016. DOI: 10.1177/0954406216650711.
3. Petrovic A, Lukic L, Ivanovic S, et al. Optimisation of tool path for wood machining on CNC machines. *Proc IMechE, Part C: J Mechanical Engineering Science*. Epub ahead of print 6 May 2016. DOI: 10.1177/0954406216648715.
4. Croccolo D, De Agostinis M and Fini S. Design of a cutting head for a crosscutting machine. *Proc IMechE, Part C: J Mechanical Engineering Science*, Epub ahead of print 20 July 2016. DOI: 10.1177/0954406216661367.
5. Shinell A, Tison T and Have HP. Structural design of s/y Dream Symphony: the largest wooden ship ever built. In: PW de Heer (ed.) *22nd international HISWA symposium on Yacht design and Yacht construction*, Amsterdam, 12–13 November 2012, pp.1–13.
6. Niemz P and Mannes D. Non-destructive testing of wood and wood-based materials. *J Cult Herit* 2012; 13S: S26–S34.
7. Crupi V, Kara E, Epasto G, et al. Prediction model for the impact response of glass fibre reinforced aluminium foam sandwiches. *Int J Impact Eng* 2015; 77: 97–107.
8. Crupi V, Epasto G, Guglielmino E, et al. Computed tomography-based reconstruction and finite element modelling of honeycomb sandwiches under low-velocity impacts. *J Sandw Struct Mater* 2014; 16: 377–397.
9. Crupi V, Epasto G and Guglielmino E. Internal damage investigation of composites subjected to low velocity impact. *Exp Tech* 2016; 50: 555–568.
10. Li W, Van den Bulcke J, Mannes D, et al. Impact of internal structure on water-resistance of plywood studied using neutron radiography and X-ray tomography. *Constr Build Mater* 2014; 73: 171–179.
11. Paris JL and Kamke FA. Quantitative wood–adhesive penetration with X-ray computed tomography. *Int J Adhes Adhes* 2015; 61: 71–80.
12. Audenino A, Crupi V and Zanetti EM. Thermoelastic and elastoplastic effects measured by means of a standard thermocamera. *Exp Tech* 2004; 28: 23–28.
13. Vergani L, Colombo C and Libonati F. A review of thermographic techniques for damage investigation in composites. *Frat Integ Strut* 2014; 27: 1–12.
14. Crupi V, Guglielmino E, Maestro M, et al. Fatigue analysis of butt welded AH36 steel joints: thermographic method and design S-N curve. *Mar Struct* 2009; 22: 373–386.
15. Maletta C, Bruno L, Corigliano P, et al. Crack-tip thermal and mechanical hysteresis in Shape Memory Alloys under fatigue loading. *Mater Sci Eng A Struct* 2014; 616: 281–287.
16. Conde MJM, Liñán CR, de Hita PR, et al. Infrared thermography applied to wood. *Res Nondestruct Eval* 2012; 23: 32–45.
17. Riggio M, Sandak J and Franke S. Application of imaging techniques for detection of defects, damage and decay in timber structures on-site. *Constr Build Mater* 2015; 101: 1241–1252.
18. López G, Basterra LA, Ramón-Cueto G, et al. Detection of singularities and subsurface defects in wood by infrared thermography. *Int J Archit Herit* 2014; 8: 517–536.
19. Berglind H and Dillenz A. Detecting glue deficiency in laminated wood – a thermography method comparison. *NDT&E Int* 2003; 36: 395–399.
20. Ludwig N, Redaelli V, Rosina E, et al. Moisture detection in wood and plaster by IR thermography. *Infrared Phys Techn* 2004; 46: 161–166.
21. López G, Basterra LA and Acuña L. Estimation of wood density using infrared thermography. *Constr Build Mater* 2013; 42: 29–32.

Appendix 1

Statistical analysis of the tensile Young modulus

A1 – Linear regression analysis of tensile data. The experimental data in terms of *applied load F* (measured in N) and *elongation* Δl (measured in mm) have been transformed in terms of nominal *tensile stress* $\sigma = \frac{F}{A_o}$ and nominal *linear strain* $\varepsilon = \frac{\Delta l}{l_o}$, where A_o is the initial cross-sectional area of the specimen and l_o is the gage length fixed by the extensometer ($l_o = 100\,\text{mm}$).

In the sample data, ε has been assumed as independent variable and σ as dependent variable.

A linear regression analysis has been performed taking into account only the data in the initial region (about in the range between 0.10 and 0.40 F_{max}).

The initial region has been chosen a sub-region in such a way to get a regression straight-line with a *coefficient of determination* $R^2 > 0.99$.

The *slope m* of the regression line so drawn represents the *Young modulus E* corresponding to the analysed test

$$m \equiv E$$

The analytical procedure is now exposed.

If the linear strain ε and the tensile stress σ are denoted by x and y, respectively, and the number of data points considered by n, the *mean* values of the x-data and the y-data are

$$\bar{x} = \frac{\sum_{i=1}^{n} x_i}{n} \quad \bar{y} = \frac{\sum_{i=1}^{n} y_i}{n}$$

The *slope* of the regression line is given by

$$m = \frac{\sum_{i=1}^{n} (x_i - \bar{x})(y_i - \bar{y})}{\sum_{i=1}^{n} (x_i - \bar{x})^2}$$

and the corresponding *coefficient of determination* R^2 is

$$R^2 = \frac{\left[n\left(\sum_i x_i y_i\right) - \left(\sum_i x_i\right)\left(\sum_i y_i\right)\right]^2}{\left[n\left(\sum_i x_i^2\right) - \left(\sum_i x_i\right)^2\right]\left[n\left(\sum_i y_i^2\right) - \left(\sum_i y_i\right)^2\right]}$$

A2 – Statistical distribution of Young modulus E. The collection of the *Young modulus* $E \equiv m$ determined for each specimen forms a series of E-data (whose number is denoted by N) which can be statistically analysed considering it a *normal* (or *Gaussian*) *distribution*.

For an E-data population normally distributed, the *probability density function pdf*(E) is so expressed

$$pdf(E) = \frac{1}{s\sqrt{2\pi}} \exp\left[-\frac{(\mathrm{E} - \mathrm{E})^2}{2\mathrm{s}^2}\right]$$

where

$\bar{E}$ is the *mean* value of the E-data population

$$\bar{E} = \frac{\sum_{i=1}^{N} E_i}{N}$$

s^2 is the *variance* (or *mean square* MS)

$$s^2 = \frac{\sum_{i=1}^{N} (E_i - \bar{E})^2}{N - 1}$$

s is the standard deviation (or root mean square (RMS))

$$\mathrm{RMS} = \sqrt{s^2} = \sqrt{\frac{\sum_{i=1}^{N} (E_i - \bar{E})^2}{N - 1}}$$

The RMS is the best index to represent the degree of dispersion within a series of results, along with the *coefficient of variation*

$$CoV = \frac{\mathrm{RMS}}{mean}$$

A3 – Characteristic Young modulus E_k. The *characteristic Young modulus* E_k of the population is assumed, in this context, as the value of E representing the *percentile corresponding to 5% probability of occurrence*, thus it is denoted by $E_{k,05}$.

In general, the *percentile* (for instance, the 5-percentile) associates with a given probability of occurrence (for instance, the 5%) is the value in the range of a set of data which separates the range itself into two groups so that the measures lying below this value have the probability of occurrence equal to the given percentage.

The *5-percentile value* for data normally distributed is so determined

$$E_{k,05} = \bar{E} - 1.645\ \mathrm{RMS}$$

where $\bar{E}$ is the mean value of the E-data set, and RMS is the standard deviation of the statistical distribution.